Measurement of Drag on a Scramjet Engine in a Shock Tunnel

K. K. N. Anbuselvan, V. Menezes[1], and K. S. N. Abhinav Kumar
Department of Aerospace Engineering, Indian Institute of Technology Bombay,
Powai, Mumbai 400076, INDIA.

Abstract
The net drag on a non-fuelled, internal compression, constant-area combustor scramjet engine was measured using a single-component accelerometer balance in a shock tunnel at a freestream Mach number of 8 and a flow total enthalpy of 1.35 MJ/kg. The flow fields of the model were simulated using a commercial CFD code in order to understand the aerodynamics of the engine and compare with the measured net drag co-efficient. Measured and computed values of the net drag co-efficient were found to be in a good agreement.

1. INTRODUCTION

Development of balances to measure forces on models in hypersonic impulse facilities can pose challenges as the forces are to be measured on fastened models within a duration of about a millisecond. The constraints involved are: making the mounted model un-restrained during the shock tunnel testing and, using fast response sensors to acquire sufficient data within a millisecond. Accelerometer balances are one of the force measurement techniques used extensively in shock tunnels, and are believed to be quite reliable when aerodynamic forces on a complex geometry are under consideration. Forces on hypersonic models in shock tunnels were successfully measured using accelerometer balances [1, 2, 3] where external aerodynamics of the body was of significance. In such cases, the balance along with the sensors was housed in a hollow, axisymmetric model (typically re-entry or missile shaped) and, the mounting sting of the model was drawn from the base of the model, keeping the mounting structure in the shadow of the model, thus avoiding its interference with the flow. But the models such as scramjet engines where the internal aerodynamics is also significant require an alternative configuration of the force balance system such that: i) the model is unrestrained during the test, ii) the sensors are housed in the model and concealed from the high speed flow to avoid disturbances in signals, and iii) the model has a mounting structure which minimally interferes with the hypersonic flow.

The present work is about measuring net drag on a scramjet engine in a shock tunnel, without fuel injection, at a freestream Mach number of 8, using a single-component accelerometer balance. The flow field of the model has been simulated using a CFD code and, the computed drag co-efficient is in good agreement with the measured one.

2. EXPERIMENTAL METHODOLOGY

2.1. Test Facility

The experiments were carried out in IITB-Shock Tunnel (IITB-ST), a schematic of which is shown in Fig. 1. The tunnel consists of a shock tube, which is 7.2 m in length and 51.5 mm in diameter. The shock tube is divided into high pressure (driver) and low pressure (driven) sections, which are separated by a metallic diaphragm, typically aluminum. During the operation, the diaphragm isolating the driver and driven sections is ruptured by pressurizing the driver section by pumping in the driver gas. The sudden rupture of the metallic diaphragm generates a shock wave that propagates through the test gas in the driven section. The test gas, which initially is at a lower pressure and room temperature, is highly compressed and heated by the propagation of the shock wave. The incident shock, on reaching the end

[1]Corresponding Author: V. Menezes, Department of Aerospace Engineering, Indian Institute of Technology Bombay, Powai, Mumbai 400076, India, Phone. +91-22-2576-7130, Fax. +91-22-25722602, E-mail. viren@aero.iitb.ac.in

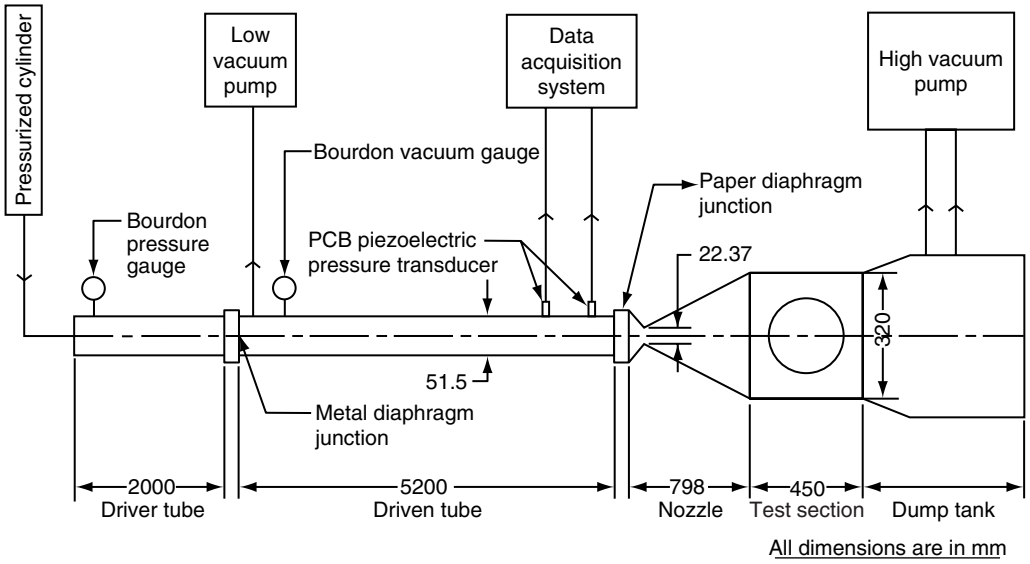

Figure 1. Schematic of the shock tunnel.

of the driven section, undergoes a total reflection and propagates back into the driven section, enhancing the pressure and temperature of the test gas further. The particle motion behind the reflected shock is almost zero, and this creates a momentary reservoir of high-pressure, high-temperature test gas at the entry to the conical shaped, converging-diverging nozzle. A very thin paper diaphragm isolates the nozzle from the driven section. The nozzle is maintained under a high vacuum before the initiation of the flow. The paper diaphragm gets ruptured due to the pressure generated by the propagating shock wave and the high-pressure, high-temperature flow at the entry to the nozzle starts expanding through the nozzle to a freestream of Mach 8 into the test section of dimensions 300 mm × 300 mm × 450 mm.

Helium and atmospheric air were the driver and test gases, respectively, for all the experiments. Two pressure sensors towards the end of the driven section, mounted 500 mm apart, were used to measure the speed of the incident shock wave and the reservoir/nozzle-supply pressure. A pressure sensor placed at the exit of the nozzle recorded the history of the Pitot pressure that was available for the test.

A typical Pitot signal for the present set of experiments is shown in Fig. 2. The signal has a rise time of 0.72 ms, which is followed by a steady trend for about 0.8 ms and after this, the trend declines. The time of the steady Pitot signal is the useful test time during the experiment. The decline in the signal can be attributed to the arrival of the expansion wave, which terminated the test time in the present case. A cross sectional area at the exit of the nozzle over which the freestream is steady was determined by the Pitot measurements, and the radius of this area from the centre of the nozzle exit was found to be about 50 mm. The freestream Mach number distribution over this area was 8 ± 4%. This indicates that the tunnel can comfortably accommodate a test model of 100 mm diameter. The freestream conditions for the tests were determined based on the recorded nozzle supply and exit pressures, assuming an isentropic expansion through the nozzle. The typical freestream conditions for the present set of experiments are given in Table 1. Flow total enthalpy and the effective test time for these experiments were 1.35 MJ/kg and 600 μs, respectively.

2.2. Test Model

The model was a scramjet engine with a mounting system and an accelerometer balance. The schematic of the model is shown in Fig. 3. The scramjet engine considered for this study was of internal-compression, constant-area combustor type that consisted of an intake, a combustion chamber and a nozzle. The engine was made of aluminum and was 389.75 mm long, 59 mm high, 50 mm wide, and weighed 1688.5 g.

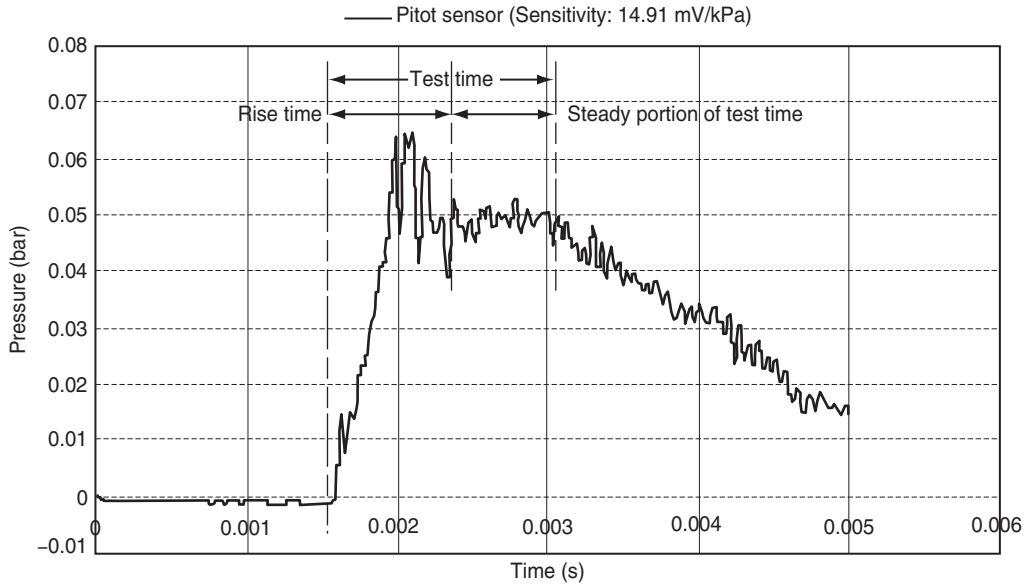

Figure 2. Time history of the Pitot pressure.

The engine was internally 2 Dimensional with a rectangular flow path, and was made of two parts; an upper part and a lower part. Each part had two ramps at the intake, initially with a convergence of 9° for a length of 83.75 mm and then with a convergence of 12° for a length of 28.25 mm. The intake was followed by a constant area combustion chamber of 50 mm width and 20 mm height for a length of 156.25 mm, which was terminated in a nozzle with a divergence angle and a length of 9° and 121.50 mm, respectively.

A slot and a C-channel were provided in the lower and upper parts, respectively, near the combustion chamber to reduce the weight of the model. The C-channel in the upper part housed the force balance with an accelerometer. The C-channel was closed with the cover plate on the top using screws as shown in Fig. 3.

The external flow over the engine was non-symmetrical due to the presence of the mounting system and an asymmetry in the external geometry of the engine. The engine was suspended from the top of the tunnel test section using a slender rhombus of 102 mm height, 20 mm length and 40° included angle, which was followed by a rubber bush based soft suspension system at its bottom that made the model unrestrained in the axial direction during the shock tunnel testing. The top surface of the engine, above the intake and the nozzle sections, had inclinations of 4.5° and 4.12°, respectively, to accommodate the accelerometer balance system. The rhombus shaped vertical mounting structure of the balance was isolated from the engine by the rubber bushes of the transverse and the axial suspension systems, as shown in Fig. 4. The mounting and the rigid structures of the balance were fabricated out of stainless steel.

Table 1. Typical test conditions in shock tunnel.

Freestream Mach number	**Total Pressure**	**Total Enthalpy**	**Freestream Density**	**Freestream Pressure**	**Freestream Reynolds Number**	**Freestream Temperature**
M_∞	P_0(MPa)	H_0(MJ/kg)	ρ_∞(kg/m^3)	p_∞(Pa)	$\frac{\mathrm{Re}_\infty}{m}$	T_∞(K)
8	0.74	1.35	0.0027	75.63	0.64×10^6	97.08

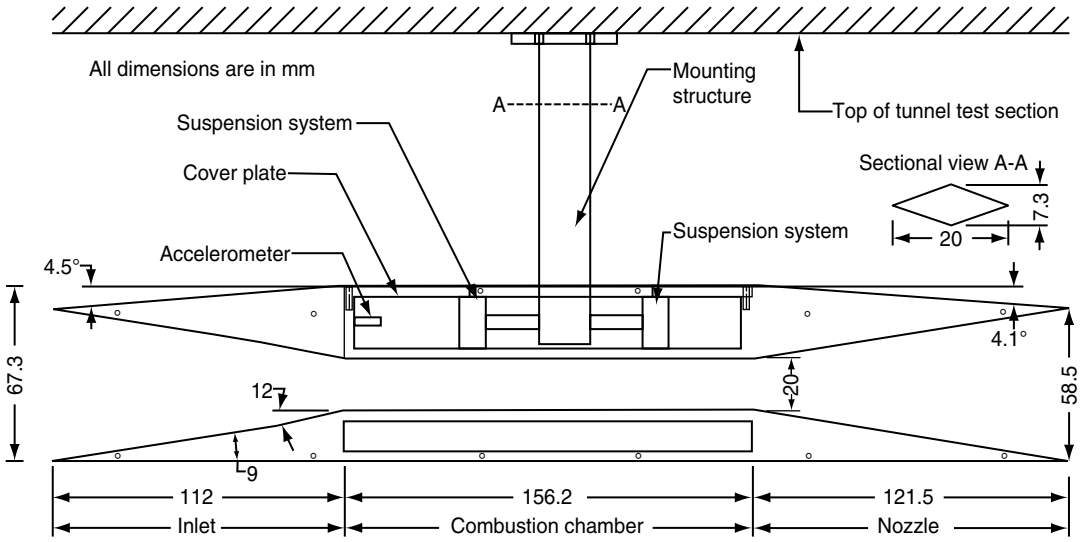

Figure 3. Schematic of the test model.

The rhombus shaped mounting structure of the model was designed based on the *hypersonic small disturbance theory*, which states that in the case of a hypersonic flow over a slender body, the change in the axial velocity due to the presence of the body is very small and is of the order of the square of the slenderness ratio of the body. The overall slenderness ratio of the rhombus is 0.36 and the change in the freestream velocity this rhombus can bring about is of the order of about 13%. In other words, the support structure disturbs (reduces) the freestream over the upper surface of the model by about 13%.

The proposed force balance had a single, uni-axial PCB-Piezotronics accelerometer, mounted in the C-channel, parallel to the axis of the engine as shown in Fig. 3. The sensitivity and the maximum operating frequency of the accelerometer were 100.5 mV/g and 10 kHz, respectively.

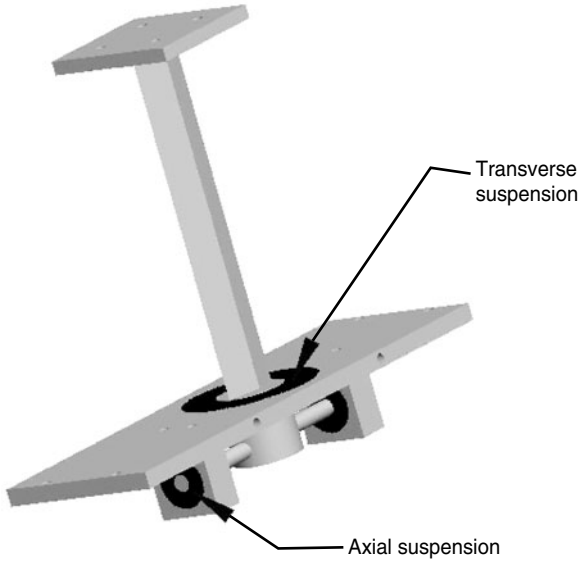

Figure 4. Suspension system for the model.

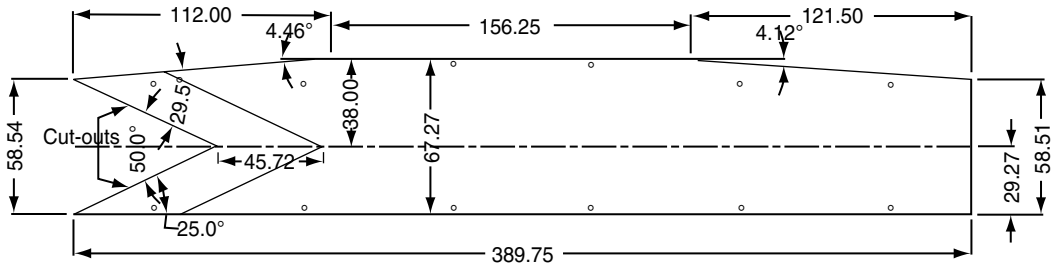

Figure 5. Side plates of the model.

The sides of the engine were covered with aluminum plates of 4 mm thickness. Cut-outs were provided in the side walls of the intake to allow a sufficient reduction in the ratio of capture to combustor-cross-sectional areas in order to facilitate the engine to self-start in the event of a non-impulsive flow environment during flight. These cut-outs had an angle of 25°, as shown in Fig. 5, which is just greater than the leading edge shock angle to prevent the spilling of the shocks. The edges of the cut-outs on the external faces of the side plates were chamfered such that they were streamlined, and all the screws were countersunk to avoid any introduction of disturbance in the flow. The internal cross-section of the model at any section was rectangular with a constant width of 50 mm.

2.3. Determination of Drag Co-efficient

The net drag force, $C(t)$ and the net drag coefficient, C_d on the model can be calculated from the following equations:

$$C(t) = m\xi \tag{1}$$

$$C_d = \left[\frac{C(t)}{q_\infty A}\right] \tag{2}$$

where, m is the mass of the model, ξ is the measured acceleration from the axial accelerometer (i.e., mean value of the signal voltage-rise in the steady state region ÷ accelerometer sensitivity), q_∞ is the freestream dynamic pressure in the tunnel test section and A is the reference area based on the frontal projected area of the engine. The net drag, which was calculated based on the measured acceleration is the difference of the total drag (i.e., the sum of pressure and viscous forces) and the thrust generated by the nozzle. The $C(t)$ and C_d calculated from the Eqs. (1) and (2) above are based on the assumption that the suspension system of the model does not offer any restraint to the motion of the model. The following equations can be used to calculate the true values of axial force $C'(t)$ and drag coefficient C'_d, taking the restraint of the suspension system into account [1].

$$C'(t) = \frac{m\xi}{1 - t^2\left[\frac{k}{2m}\right]} \tag{3}$$

$$C'_d = \left[\frac{C'(t)}{q_\infty A}\right] \tag{4}$$

where, t is the test time and k is the stiffness of the suspension system.

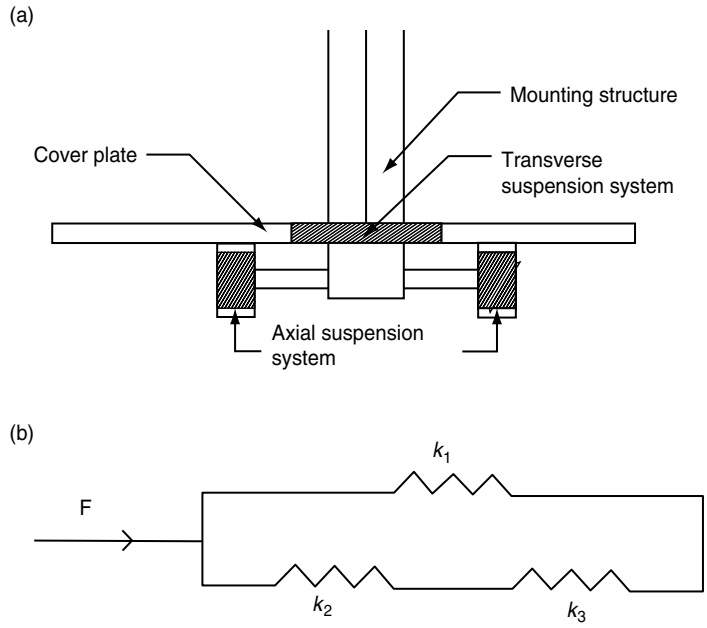

Figure 6. a) Suspension system for the model. b) Spring analogy of the suspension system.

Stiffness of rubber bushes of the transverse suspension, k_1 and the axial suspensions, k_2 and k_3, were determined through uni-axial compression tests on an Universal Testing Machine and the values were found to be 31.9 N/mm, 8.22 N/mm, and 8.22 N/mm, respectively. The suspension system shown in Fig. 6(a) can be transformed into a spring analogy as in Fig. 6(b), and the equivalent stiffness of the combined suspension system can be calculated using Eq. (5), and the value of the equivalent stiffness in the present case is calculated to be 10.85 N/mm.

$$k = \frac{k_1(k_2 + k_3)}{k_1 + k_2 + k_3} \tag{5}$$

Since the difference between $C(t)$ and $C'(t)$ for an average test time of 600 μs was found to be 0.115%, which is negligible, the values obtained through Eqs. (1) and (2) were used for further analysis.

3. NUMERICAL SIMULATION

The flow fields of the model were simulated using a commercial CFD code *Fluent 6.3*, in order to understand the aerodynamics of the engine and to compare with the measured net drag coefficient. The internal flow field of the engine is characterized by boundary layer separation and re-attachment processes that could create local pockets of turbulent flow. Hence, a turbulence model (Spalart-Allmaras) was used to simulate the turbulent flow behaviour. The external flow field of the model was assumed to be laminar as the Reynolds number based on the model length was well below the limit of hypersonic transition. Therefore, the test model was split into four parts and the simulations on different parts were carried out separately in order to save the computational memory and time. The four simulations carried out are as below:

1) Internal flow in the engine solving 3-D Navier-Stokes equations, incorporating Spalart-Allmaras turbulence model.
2) External flow over the top surface of the engine with the rhombus shaped vertical mounting structure, solving 3-D Navier-Stokes equations. Flow was assumed to be laminar.

3) External flow over the bottom surface of the engine solving 2-D Navier-Stokes equations. Flow was assumed to be laminar.
4) External flow over the side surfaces of the engine solving 3-D Navier-Stokes equations. Flow was assumed to be laminar.

Boundary conditions used in these simulations were based on the experimental test conditions. At the walls, no-slip and adiabatic conditions were used. A structured gird was generated in the computational domain using *Gambit* grid generator. A coupled solver was used to solve the governing equations with the second-order, implicit, upwind discretization scheme in the flow domain. The values of total drag co-efficient, C_d, and skin-friction drag co-efficient, C_f were monitored and the solution was deemed to be converged when these values were constant for a number of iterations.

4. RESULTS & DISCUSSION

Figure 7 shows a signal, which is the axial acceleration of the model when it encountered a free stream of Mach 8 in the test section of the tunnel. This signal is the output of the axial accelerometer mounted in the model. The signal has a gradual rise for about 0.4 ms and then is steady for 0.4 ms. The mean magnitude of the model acceleration is read on the steady part of the signal, over 0.4 ms. Figure 7 also comprises a Pitot signal which indicates the quality of the free stream in the tunnel test section. The acceleration signals of two identical shots are presented in Fig. 8, to indicate the repeatability of the test. Several tests were conducted and a good repeatability has been found in the signals. The measured, net drag co-efficient C_d, based on the frontal projected area of the model is 0.3187 and found to lie within a standard deviation of 0.00279. The measured and computed values of net drag co-efficient C_d, are compared as in Fig. 9. The difference between the measured (mean) and the computed values is found to be about 8.71%. The accelerometer signals presented in Figs. 7 & 8 exhibit some oscillations that can be attributed to the vibration of the rubber bushes on which the model was suspended, and also to the vibrations generated in the tunnel during its operation, such as diaphragm rupture etc., which did not get damped within the test time.

Figure 10 presents the total drag co-efficient over different parts of the model, based on simulations. As the model/geometry was assumed to be in a state of flight at Mach 8, the pressure acting on the surfaces of the nozzle produced a small thrust [5], which is indicated in terms of negative drag coefficient (F) in Fig. 10. The computed net drag co-efficient on the model was found to be 0.3464. The

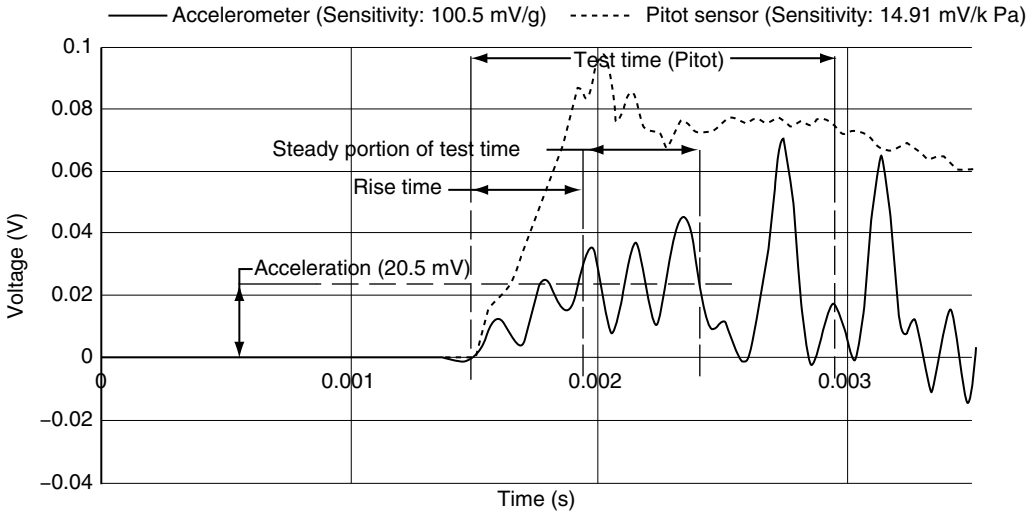

Figure 7. Model axial acceleration signal along-with the Pitot signal to indicate the test time in the tunnel.

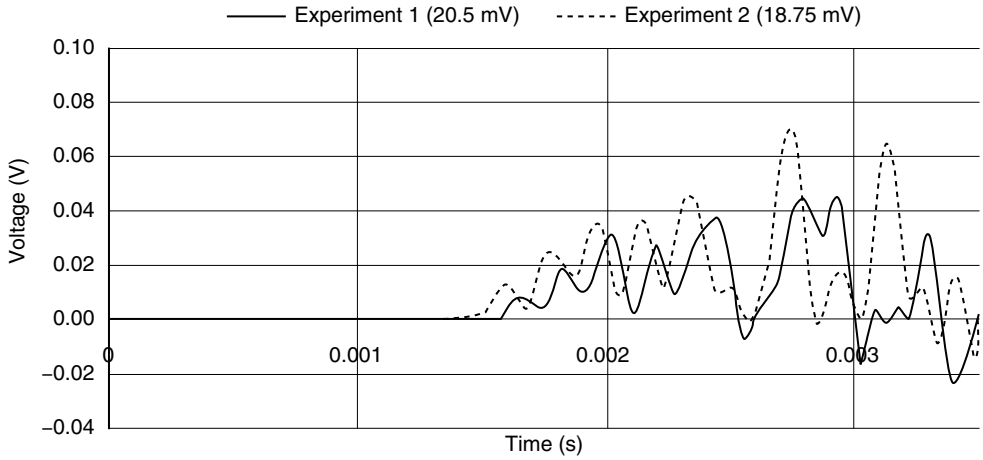

Figure 8. Axial acceleration signals indicating repeatability of the test.

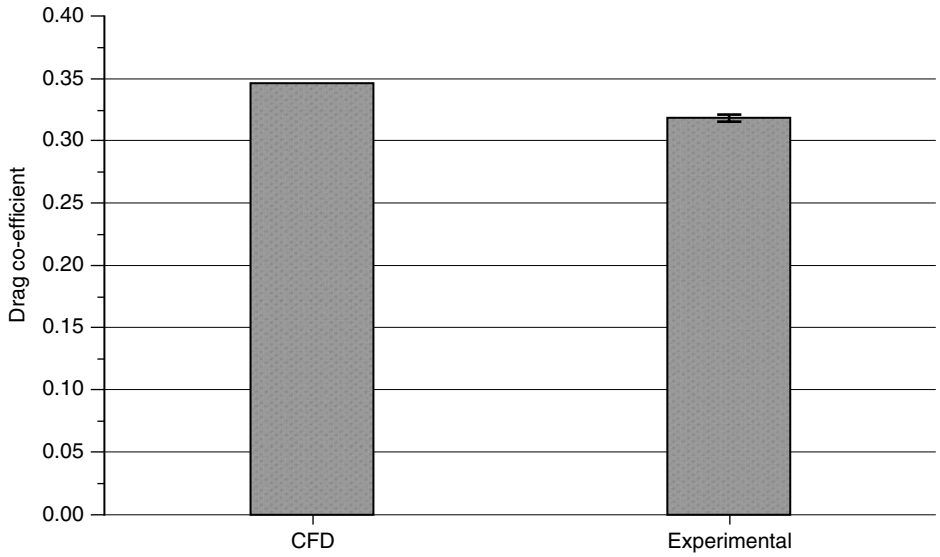

Figure 9. Comparison of measured and computed values of total drag coefficient.

total skin friction drag on the model was about 75% of the total drag, and nearly 43% of the total skin friction drag was produced by the internal surfaces of the combustion chamber. About 50% of the net drag on the model was generated by the external surfaces, which is commensurate with what has been reported in [6], out of which 88% was viscous drag and, 12% was wave drag, which is attributed to the inclinations provided on the upper, external surface. The thrust produced by the nozzle could overcome 27% of the total drag on the model.

The pressure contours along the length of the engine (internal) are shown in Fig. 11. The intake is characterized by oblique shocks generated at the ramps and the interactions of these shocks. The growth of the boundary layer along the walls is evident from Mach contours shown in Fig. 12. The adverse pressure gradient offered by the leading edge refracted shocks causes the boundary layer flow to separate and form a re-circulation bubble of 27.5 mm length at the wall down the 12° ramp. The flow gets reattached in the combustion chamber downstream.

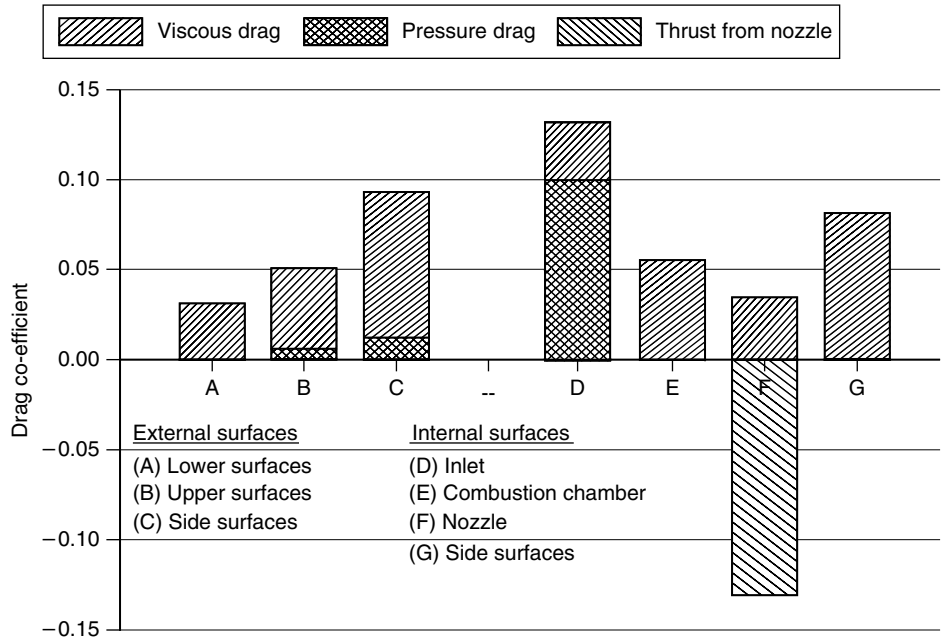

Figure 10. Drag coefficient for different components of the scramjet engine.

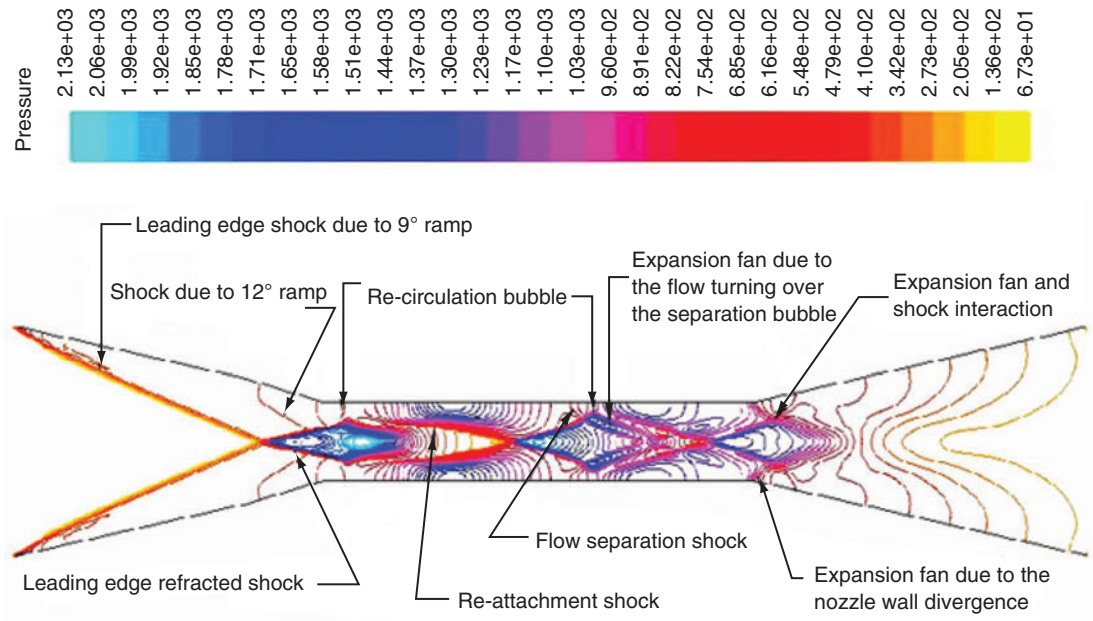

Figure 11. Simulated internal flow field (Pressure contours) of the engine.

Due to the flow separation, an oblique shock is generated upstream of the recirculation bubble, which interacts with the leading edge refracted shocks. The inviscid flow turns away from itself as it negotiates the re-circulation bubble and the expansion waves are generated in the process. Subsequently, the combustion chamber flow is characterized by shock-boundary layer interaction, shock-shock interaction and expansion fan-shock interaction. Finally, the flow is expanded through a diverging nozzle.

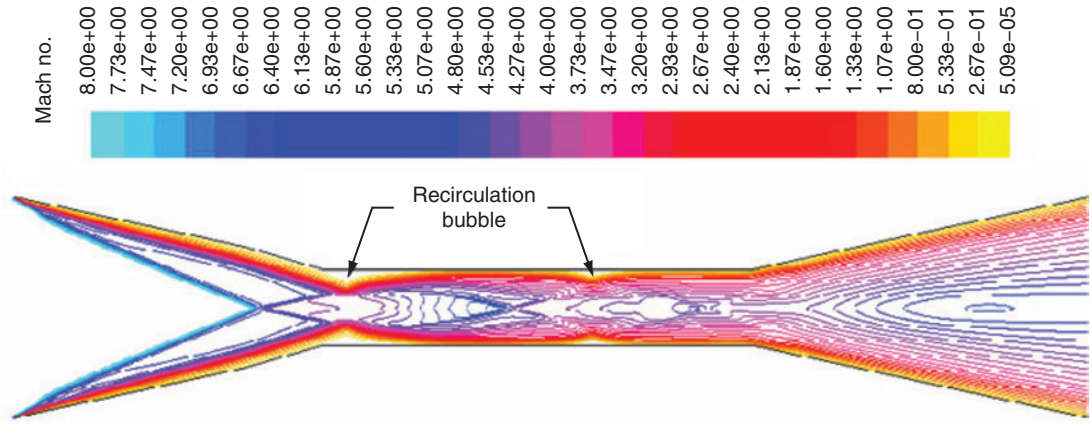

Figure 12. Mach contours of the internal flow field.

5. CONCLUSION

Drag measurements were carried out on a scramjet engine, without fuel injection, using an accelerometer balance in a shock tunnel at Mach 8. The suspension system of the model was designed in such a way that the model was minimally restrained during the test in the tunnel. The mounting structure of the model was appropriately shaped such that its interference with the flow was minimum. Numerical simulations of the flow fields of the model were carried out to have an understanding of the flow physics, and to compare the measured net drag coefficient. The experimental results are found to be in a good agreement with the computed values with a difference of about 8.71%.

REFERENCES

[1] N. Sahoo, D. R. Mahapatra, G. Jagadeesh, S. Gopalakrishnan, and K. P. J. Reddy. Design and analysis of a flat accelerometer-based force balance system for shock tunnel testing. *Measurement: Journal of the International Measurement Confederation*, 40(1): 93–106, 2007.

[2] V. Menezes, S. Saravanan, G. Jagadeesh, and K. P. J. Reddy. Experimental investigations of hypersonic flow over highly blunted cones with aerospikes. *AIAA Journal*, 41(10): 1955–1966, 2003.

[3] R. Joarder, and G. Jagadeesh. A new free floating accelerometer balance system for force measurements in shock tunnels. *Shock Waves,* 13(5): 409–412, 2004.

[4] J. D. Anderson Jr. *Hypersonic and High Temperature Gas Dynamics 2nd Edition*, AIAA Inc.,Virginia, 2006.

[5] K. Tanimizu, D. J. Mee, R. J. Stalker, and P. A. Jacobs. Drag force on quasi-axisymmetric scramjets at various flight Mach numbers: Theory and experiment. *Shock Waves,* 19(2): 83–93, 2009.

[6] T. Mitani, T. Kanda, T. Hiraiwa, Y. Igarashi, and K. Nakahashi. Drags in scramjet engine testing: Experimental and computational fluid dynamics studies. *Journal of Propulsion and Power*, 15(4): 578–583, 1999.